12th IFAC International Symposium on
Advanced Control of Chemical Processes
July 14-17, 2024. Toronto, Canada

A Modular Soft Sensor for Centrifugal Pumps

Sebastian Leonow * **Qi Zhang** ** **Martin Mönnigmann** ***

* *(e-mail: sebastian.leonow@ruhr-uni-bochum.de)*
** *(e-mail: Qi.Zhang-x92@ruhr-uni-bochum.de)*
*** *(e-mail: martin.moennigmann@ruhr-uni-bochum.de)*
Automatic Control and Systems Theory, Department of Mechanical Engineering, Ruhr University Bochum, Universitaetsstrasse 150, 44801 Bochum, Germany.

Abstract: Soft sensors experience an increasing interest in recent years, as they can replace expensive hardware meters and the required embedded computing hardware has become cheap and powerful. We report results for the implementation of a soft sensor for the flow rate estimation in centrifugal pumps that achieves root mean square errors of about 5%. The proposed soft sensor is based on generic models for the drive and hydraulic part of the pump to ensure widespread applicability. We show the soft sensor and the models it is based on can be parametrized with simple measurements. All theoretical considerations are corroborated with measurements on a real industrial pump in a laboratory setup. The results show that the proposed soft sensor is capable of providing reliable flow rate estimates in spite of plant model mismatch and uncertain hardware components.

Keywords: Soft Sensor, Flow Rate Estimation, Centrifugal Pump, Variable-Speed Drive.

1. INTRODUCTION

Pumps are ubiquitous devices and their importance for chemical engineering processes is evident. Pumps consume nearly 22% of the electromotoric energy on a global scale (Arun Shankar et al., 2016). In particular centrifugal pumps account for 16% of the global electromotoric consumption, leveraging already minor efficiency improvements to an immense long-term impact. Modern centrifugal pumps are generally optimized to a certain operating point, where the efficiency approaches up to 94% in certain setups (Elsey, 2023). Operating the pump at or near its best efficiency point (BEP) results in the lowest energy consumption and reduced operational costs, but this is only possible if the current operating point is known. Hardware flow meters are traditionally employed to measure the operating point, however, have the obvious drawbacks of being expensive, difficult to maintain, and sometimes impossible to install into an existing setup (Doraiswami and Cheded, 2014; Martin et al., 2021). Soft sensors have become a relevant alternative in recent years, as they typically need only easy to acquire measurements, and a mathematical system model to infer the operating point or parameters of the plant (Wang et al., 2009; Leonow and Mönnigmann, 2013). Since obtaining a comprehensive and accurate first principles model is generally challenging due to the complexity of a pump system with a large number of uncertain parameters, pump manufacturers use data-driven models, which are easily parameterized during the scheduled test stand runs of newly manufactured pumps (Leonow and Mönnigmann, 2013). While many recent academic results and laboratory and field tests of soft sensors with different and improved approaches are available (e.g., Leonow and Mönnigmann, 2016; Lima et al., 2022; Wu et al., 2023), the commercial availability of ready-to-use soft sensors is limited to a very few, mainly from large pump manufacturers (Pauly, 2011). One important factor for this discrepancy of laboratory to real-world applications is the inhomogeneous nature of pump installations, where pump and electric drive usually come from different manufacturers and are finally assembled on-site (cf. Fig. 1). Consequently, the pump manufacturer, who usually offers and parameterizes the soft sensor, is not able to take precise models for motor and plant into account. The resulting plant model mismatch can lead to a significant inaccuracy of the soft sensor that would require a complete re-design, in particular when a data-driven model is used. This re-design can usually not be accomplished by the pump user, due to a lack of equipment and knowledge.

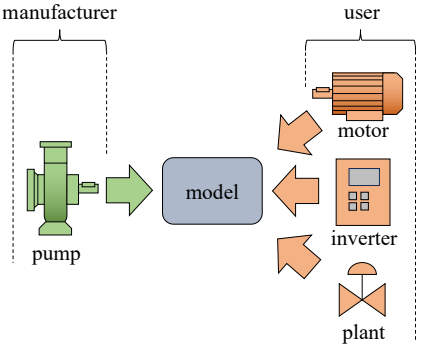

Fig. 1. Model parameterization split between pump manufacturer and user to reduce plant model mismatch.

⋆ Funding by the German Federal Ministry for Economic Affairs and Energy is gratefully acknowledged.

The aim of this work is twofold. First, we develop a component-wise, holistic model to address the uncertainty that is introduced by assembling the pump system on site with components from different manufacturers and by the hydraulic plant itself. Second, the model must be simple enough for the pump user to adapt it to the current plant setup. We introduce the modeling and parameterization in Section 3, followed by a performance evaluation in a standard soft sensor setup based on the Unscented Kalman Filter in Section 4.

2. NOTATION AND PRELIMINARIES

We introduce i as the effective stator current of the motor (in A), P as the motor and pump mechanical power and P_{el} as the electrical power (in W), q as the actual flow rate (in m^3/h), n as the rotational speed (in 1/min), f as the frequency of the electrical current (in Hz), and M as the torque (in Nm). Indices min and max denote the corresponding intervals that represent the respective operating ranges, e.g. $i \in [i_{\min}, i_{\max}]$. The index 0 indicates a nominal value, i.e. a value that is associated to the nominal, or intended operation of the pump.

Pumps and motors are characterized by various input-output relations, also known as characteristics. For example, for a given rotational speed n, the $P \to i$ characteristic describes the effective stator current i of a motor as a function of the mechanical power P.

2.1 Hydraulic affinity laws and energy balances

Hydraulic affinity laws are fundamental principles that describe how changes in key parameters affect the performance of hydraulic systems. The hydraulic affinity laws allow a transformation of characteristics to different rotational speeds and therefore reduce the amount of data to be measured for modeling a pump system. We will use the scaling laws

$$q = q_0 \cdot \frac{n}{n_0} \ , \quad P = P_0 \cdot \left(\frac{n}{n_0}\right)^3 \cdot \frac{\eta_P}{\eta_{P,0}} \tag{1}$$

for flow rate q and mechanical power P, respectively (Gülich, 2010, p. 134).

In addition to the affinity laws, we will use simple energy balances of mechanical and electrical energy

$$P = M \cdot n \cdot \pi \cdot (30)^{-1} \ , \quad P_{\text{el}} = U \cdot i \ . \tag{2}$$

3. COMPONENT WISE MODELLING

The components of a typical pump system are depicted in Fig. 1. We aim to develop a model structure reflecting this setup, resulting in a model structure as depicted in Fig. 2. We claim that the underlying assumption on the specific pump system setup will hold for a wide range of real-world systems. The input to the model is the frequency setpoint f which determines the amplitude and frequency of the voltage U provided to the motor. The frequency is the primary control input of the pump system. The motor current i, which is assumed to be measured by the inverter, will be used as the primary measurement for the soft sensor.

The motor is coupled to the pump via a stationary coupling, therefore torque M, rotational speed n, and the resulting mechanical power P are equal for pump and motor. The flow rate q is obviously affected by the pump. However, the flow rate does not only depend on the pump type and operation, but it results from the interaction of the pump with the hydraulic plant it is connected to. Since the actual plant is usually unknown during the design phase of a soft sensor (carried out by the pump manufacturer before the actual plant is known), and since the pump characteristics are theoretically independent of it (Gülich, 2010, pp. 665), the plant is often excluded from the model. However, secondary effects like vortices at the inlet or cavitation have shown to significantly influence the pump efficiency and affect its characteristics (Gülich, 2010, pp. 687). Therefore, it is worth considering the plant to improve the soft sensor performance (see Sec. 3.4 and Fig. 6).

We summarize the modeling assumptions in the following subsections. We try to assume the most widespread setup of the modeled components to ensure a wide range of applications.

3.1 Inverter model

In open loop mode, the inverter receives the frequency setpoint, for example from an external source, and supplies electrical current with the desired frequency to the motor. The output voltage U depends on the frequency f and is defined in the inverter parameters. Typical functions $U(f)$ are linear or quadratic, usually chosen according to the power demand of the machine that is connected to the motor. A quadratic function $U(f)$ is common for pumps. We therefore implement

$$U(f) = U_0 \cdot \left(\frac{f}{f_0}\right)^2 \tag{3}$$

as inverter model, with the supply grid voltage U_0 and the supply grid frequency f_0 as parameters. We omit the case of non-quadratic $U(f)$ functions here but note that the corresponding parameters can usually be acquired easily from the inverter user interface.

The inverter also serves as a sensing device, as it usually monitors the motor current. It depends on the inverter if the apparent current or the true current is measured, which we will address in the motor modeling in section 3.2. Independent from the type of measurement we can assume that it undergoes a lowpass filtering, and condense

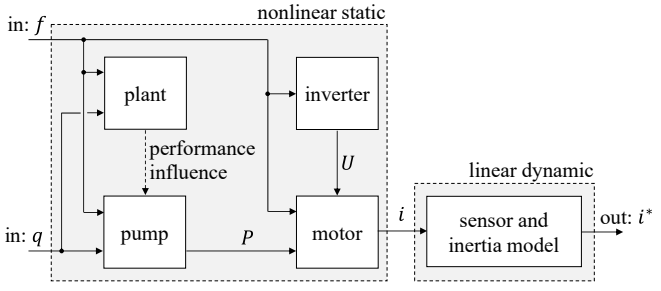

Fig. 2. The model structure reflects the connections between the real pump system components.

all dynamics of motor, pump, and current sensors into one first-order, linear dynamic model

$$\frac{\mathrm{d}i^*(t)}{\mathrm{d}t} = -\frac{1}{T_c}\cdot i^*(t) + \frac{1}{T_c}\cdot i(t)\ , \tag{4}$$

where $i(t)$ results from the steady state model and i^* is the measured current. The parameter T_c in (4) holds the combined lag time of the response of $i^*(t)$ on a change in $i(t)$, respectively $f(t)$, and can be identified from a step response measurement or even set equal to the filter time constant of the inverter. For large pumps with a significant inertia of the rotating components, a more elaborate model for (4) may be required (Leonow and Mönnigmann, 2016).

3.2 Motor model

We assume a squirrel cage asynchronous motor, because it is the most common drive type for pumps. We introduce a set of motor parameters for the established steady-state models, from which we eventually derive a simplified, easier-to-parameterize model. We introduce the indices 1 and 2 for stator and rotor, and the parameters R and L for resistance and inductivity, respectively, of the motor windings. L_M describes the mutual inductance, z_p is the number of pole pairs, and the leakage coefficient $\sigma = 1 - L_M^2(L_1L_2)^{-1}$. The nominal mechanical power P_0 marks the design operating point. We consider $0.5P_0 < P < 1.5P_0$ as normal operating range in the following. Following Schröder (Schröder, 2013, pp. 247), torque M and current i of an asynchronous motor in steady state are

$$M = k_M\cdot\frac{U^2}{f^2}\cdot\frac{s\cdot s_B}{s_B^2+s^2} \tag{5}$$

$$i = k_i\cdot(-j)\cdot\frac{U}{f}\cdot\frac{\sigma\cdot s_B + js}{s_B+js}\ , \tag{6}$$

where $s = (f - nz_p60^{-1})f^{-1}$ is the motor slip, $s_B = R_2(f\sigma L_2)^{-1}$ is the breakdown slip, and $k_i = (\sigma L_1)^{-1}$ is constant for a given motor. The factor $k_M = 2M_B$ in (5) holds the breakdown torque M_B, i.e. the maximal torque the motor can provide. The breakdown torque scales with $(U/f)^2$, which we included in (5), and is otherwise constant for a given motor:

$$M_B = \frac{3}{4}\cdot z_p\cdot\frac{L_M^2}{\sigma L_1^2 L_2}\ .$$

The primary connecting variable between motor and pump is the mechanical power $P = M\cdot n\cdot\pi\cdot(30)^{-1}$, which, with $n = (1-s)f\cdot 60\cdot(z_p)^{-1}$ and (5), can be expressed via

$$P = k_P\cdot\frac{U^2}{f^2}\cdot\frac{s(1-s)}{s_B^2+s^2}\ , \tag{7}$$

where $k_P = M_B\cdot(3600\pi R_2)\cdot(z_p\sigma L_2)^{-1}$ is constant. Solving (7) for s yields

$$s = \pm\frac{\sqrt{-4s_B^2\tilde{P}^2 - 4s_B^2\tilde{P}+1}\pm 1}{2(\tilde{P}+1)} \text{ with } \tilde{P} = \frac{P}{k_P}\cdot\frac{f^2}{U^2}\ . \tag{8}$$

The motor current (6) is complex valued and it depends on the inverter how i is measured (see Sec. 3.1). If the inverter measures the true current, i.e. $\Re(i)$, (6) simplifies to

$$\Re(i) = k_i'\cdot\frac{U}{f^2}\cdot\underbrace{\frac{s}{s_B^2+s^2}}_{i_R} \tag{9}$$

with constant $k_i' = \frac{R_2(1-\sigma)}{\sigma^2 L_1 L_2}$. In case the apparent current $|i|$ is measured, (6) becomes

$$|i| = k_i''\cdot\frac{U}{f^2}\cdot\underbrace{\sqrt{\frac{\sigma^2+s^2/s_B^2}{s_B^2+s^2}}}_{i_A} \tag{10}$$

with constant $k_i'' = \frac{R_2}{\sigma^2 L_1 L_2}$. Inserting s from (8) into i_R in (9) and i_A in (10) yields the map $P \to i$ for given U and f. The shape of this map depends on s_B and σ only, since all remaining terms in (8), (9), and (10) are constant scaling factors, independent of P. This allows for a general statement regarding nonlinearity concerning s_B and σ. We introduce the relative nonlinearity measure proposed by Emancipator and Kroll (1993), which quantifies the fitness of a least squares optimal linear approximation $y = a\cdot x + b$ of a nonlinear function $f(x)$ via

$$\lambda = \frac{\sqrt{\int_{x_{\min}}^{x_{\max}}\left(f(x) - a\cdot x - b\right)^2\mathrm{d}x}}{\left(\max\left(f(x)\right) - \min\left(f(x)\right)\right)\sqrt{x_{\max}-x_{\min}}} \tag{11}$$

over an interval $x_{\min} \le x \le x_{\max}$. Applying (11) to (9) and (10) with least squares optimal linear fits yields the results depicted in Fig. 3, where we chose typical ranges for $s_B \in (0, 0.3)$ and $\sigma \in (0.1, 0.5)$, and varied s in the nominal operating range between $0.25s_B$ and $0.5s_B$.

Evidently, i_R shows a very linear behavior and stays well within the 2.5% limit proposed by Emancipator and Kroll (1993), while i_A shows a higher nonlinearity, in particular for larger values of σ. We investigated several motor parameters from various sources (e.g., Schröder, 2013; Allirani, 2009; Benheniche and Bensaker, 2015) in the power range from 0.75kW to 180kW, which all had $\sigma, s_B < 0.18$, supporting the linear modeling approach also for i_A. Nevertheless, for particular motors, a more elaborate approach may be required.

Figure 4 depicts $\Re(i)$ and $|i|$ over P, which result from inserting (8) into (9) and (10), respectively, for sample motor parameters from Schröder (2013). The idle current $\Re(i(P=0))$ is either 0, as $i_R(0) = 0$, while $|i(P=0)|$ scales with U, as $i_A(0) = \sigma$. Both $\Re(i)$ and $|i|$ show a reasonably linear shape in the nominal operating range. The relative nonlinearity (11) is 0.2% for $\Re(i)$ and 2.1% for $|i|$, so well below 2.5%. The slope of the linear approximation scales with $(1/U)$, which follows directly

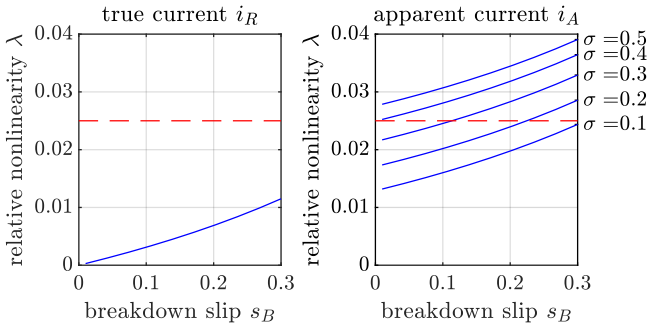

Fig. 3. The blue curves depict λ from (11) applied to i_R from (9) and i_A from (10), evaluated over s_B and σ. The red dashed line indicates a relative nonlinearity of 2.5%.

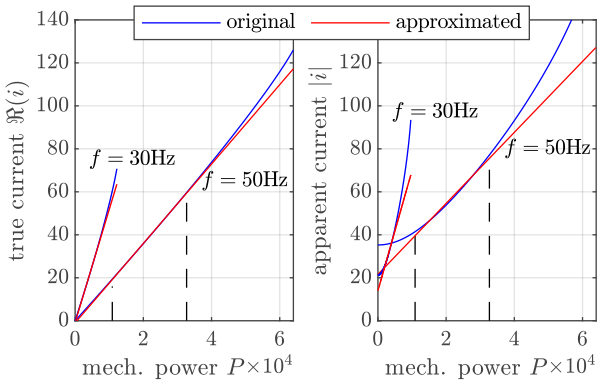

Fig. 4. The blue curves depict $\Re(i)$ and $|i|$ over P resulting from (8), (9), and (10), for two situations with ($f = 50$Hz, $U = 380$V) and ($f = 30$Hz, $U = 137$V). The red lines result from best fitting linear approximations in the considered operating range $0.5P_0 < P < 1.5P_0$.

from the influence of U and f implied in (8), (9), and (10), which also coincides with the fundamental power balances stated in (2). It is important to note that none of the motor parameters affect the scaling implied by U and f.

Considering the above observations, we propose a universal linear model

$$i(U,P) = b_{i,0} \cdot \frac{U}{U_0} + m_{i,0} \cdot \frac{U_0}{U} \cdot P \ , \tag{12}$$

where idle current $b_{i,0}$ and current slope $m_{i,0}$ correspond to the nominal operation at f_0 and can be parameterized by a simple measurement of the current, by characteristics from the maintenance manual, or ultimately even by using the datasheet or motor type plate. The last option will yield the most uncertain parameters since the idle current is usually not given.

3.3 Pump model

The hydraulic part of the pump system is within the scope of the pump manufacturer, who usually has sufficient measuring equipment to measure pump characteristics. With data for the $q \to P$ characteristic for nominal frequency f_0 and the scaling laws (1), a polynomial approach

$$P(f,q) = \left(\frac{f}{f_0}\right)^3 \cdot \frac{\eta_P(f)}{\eta_{P,0}} \cdot \sum_{k=1}^{m} \left(c_{p,k} \cdot \left(q \cdot \frac{f_0}{f} \right)^k \right) \tag{13}$$

maps q to P for variable frequencies f, where the required polynomial order m depends on the complexity of the $q \to P$ characteristic, and c_p are the corresponding polynomial coefficients. The parameterization of $\eta_P(f)$ requires an additional measurement for different frequencies f, captured e.g. in a polynomial or piecewise linear function. We again claim that $\eta_P(f)$ can be parameterized easily by the pump manufacturer, e.g. during a routine release measurement on a test bench.

Note that we used the inverter frequency setpoint f instead of the real speed n in (13) since n is usually not measured. However, one can reason that, if the on-site setup is well designed in terms of motor and pump dimensioning, the encountered slip s, i.e. the error introduced by replacing n with f, is similar compared to the test stand measurement and therefore already incorporated in $\eta_P(f)$.

3.4 Plant model

The plant is the most uncertain part of the design process of a soft sensor since the actual on-site setup of the hydraulic process surrounding the pump is usually not known to the pump manufacturer, in particular when pumps are interchanged or reused. Consequently, the plant is commonly excluded from the soft sensor model. The isolated modeling of the pump system is supported by the theory to a certain extent, which allows for an estimation of q based on known n and i, without including the surrounding process except for its obvious influence on q. In real-world application, however, secondary effects like inlet vortices, cavitation, or underdimensioned piping lead to a considerable change in the pump characteristics (Lin et al., 2020; Gülich, 2010) which, when not considered, will degrade the soft sensor performance significantly.

Capturing the plant influence to its full extent is elaborate and will usually require case-specific, detailed modeling, as performed by Lin et al. (2020), for example. We limit the scope here to the frequent effect of cavitation, which arises, for example, due to underdimensioned piping or false operating points, and provide a heuristic model which allows the user to adapt the parameters for a specific plant.

Cavitation usually leads to a sudden drop in the power demand of the pump, as it fails to build up pressure. We propose a heuristic model based on observations on several pumps and results from the literature (Cao and Mao, 2019; Al-Obaidi, 2019), which yields a corrected pump power $P^* = P - P^-$ with P from (13) and

$$P^- = P_{\text{cav}} \frac{f^3 \eta_P}{f_0^3 \eta_{P,0}} \left(1 + \tanh\left(\left(q\sqrt{\frac{f_0}{f}} - q_{\text{cav}} \right) c_{\text{cav}} \right) \right) , \tag{14}$$

where q_{cav} is the flow rate where cavitation starts influencing the power for $f = f_0$, and P_{cav} follows as the corresponding power P at $q = q_{\text{cav}}$. The factor $c_{\text{cav}} \ll 1$ scales the onset of the cavitation effect, where lower values lead to a smoother onset.

3.5 Parameterization and performance

We parameterize the separate models from the previous sections 3.1 to 3.4 individually, using test stand and datasheet information for a 7.5kW standard industrial pump in a hydraulic test stand, depicted in Fig. 5. For

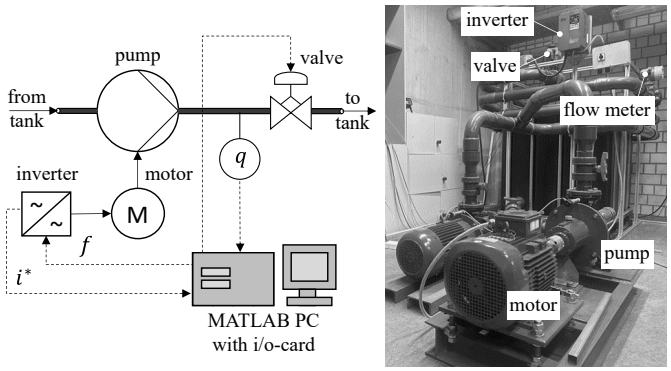

Fig. 5. Laboratory test setup with a 7.5kW standard industrial pump.

the inverter, the required parameters can be read from the operator interface. They are $U_0 = 380\text{V}$, $f_0 = 50\text{Hz}$, and a quadratic U/f-curve, as assumed in (3). Regarding the dynamic model part (4), the inverter has a filter time constant $T_c = 0.5$ seconds and measures the apparent current $|i|$. For simplicity, we will use i for $|i|$ in the following.

The motor model (12) requires the idle current $b_{i,0}$ and the slope $m_{i,0}$ of the current over P. We acquired the idle current from a no-load test resulting in $b_{i,0} = 2.3\text{A}$. The current slope was identified using the motor datasheet, which states nominal power $P_{\text{nom}} = 7.5\text{kW}$ and nominal current $i_{\text{nom}} = 14\text{A}$, resulting in $m_{i,0} = (i_{\text{nom}} - b_{i,0})/P_{\text{nom}} = 0.0016\text{A/W}$. Figure 6 depicts the results of the combined inverter and motor models in the upper left diagram, compared against test stand measurements. Sufficient model accuracy is evident for all depicted frequencies and over the whole measured power range, which is confirmed by the lowest root mean squared error (RMSE) of 0.1A for 50Hz, and the highest RMSE of 0.34A for 20Hz, which is 2.5% when compared to the nominal current $I_{\text{nom}} = 14\text{A}$. The results support the linear modeling approach proposed in section 3.2.

The polynomial part of the pump model (13) was parameterized using the datasheet provided by the manufacturer, which holds the $q \to P$ characteristic for the nominal operation at $f_0 = 50\text{Hz}$. We chose a 4th-order polynomial, depicted as the black curve in the upper right diagram in Fig. 6. The efficiency factor $\eta_P(f)$ was measured at the test stand by comparing the model to the measured P for frequencies 20 to 50Hz, at $q = 0\text{m}^3/\text{h}$, resulting in a decreasing efficiency from $\eta_P(50)/\eta_{P,0} = 0.98$ for 50Hz to $\eta_P(50)/\eta_{P,0} = 0.64$ for 20Hz. As discussed in Sec. 3.3, $\eta_P(f)$ also holds the difference in the motor slip between the datasheet measurement and our test stand measurement, which leads to the unexpected nominal efficiency $\eta_P(50)/\eta_{P,0} < 1$.

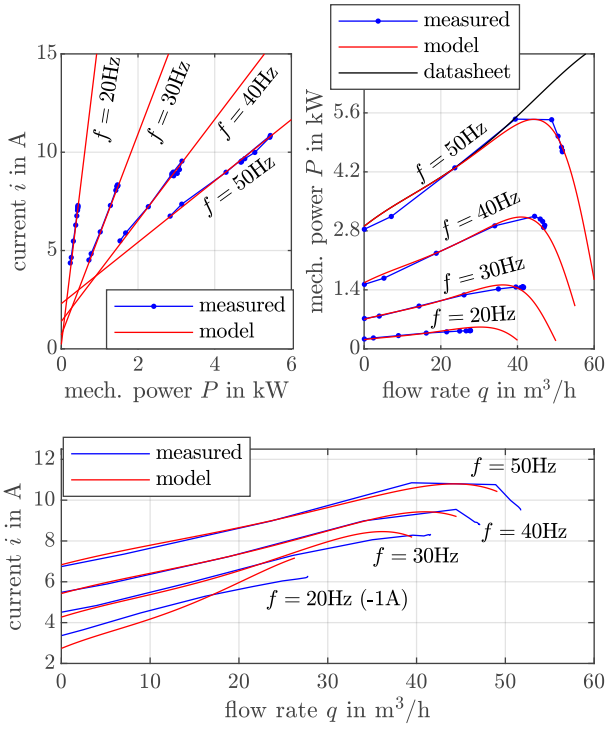

Fig. 6. Combined models against test stand data. Upper left: Inverter and motor, $P, f \to i$. Upper right: Pump and plant, $q, f \to P$. Lower: Full pumpset, $q, f \to i$.

Finally, the cavitation model required a single test stand measurement at 50Hz with a manually adjusted flow rate, revealing a cavitation onset at $q_{\text{cav}} \approx 60\text{m}^3/\text{h}$, and an according $P_{\text{cav}} = 5.5\text{kW}$. We chose $c_{\text{cav}} = 0.1$ manually by comparing the model output to the measured P.

Figure 6 depicts the combined pump and cavitation model results in the upper right diagram, where, again, a sufficient accuracy is evident. The significant difference between the datasheet characteristic (i.e. the black curve) and the measured P (in blue) is noteworthy, as this would lead to a severe model error if the plant influence was neglected. The combined pump and cavitation model yields the highest RMSE of 76.5W for 50Hz and the lowest RMSE of 58.6W for 20Hz. Compared to the maximal power P_{cav} for each frequency, the relative RMSE is below 5% for 30 to 50Hz, but increases to 13.5% for 20Hz. Further tuning of $\eta_P(f)$ can reduce this relative error but also requires more elaborate measurements. We leave $\eta_P(f)$ here as is and evaluate the impact of the model errors on the soft sensor performance in the following section.

The lower plot in Fig. 6 depicts the full pumpset model, i.e. the combination of (3), (12), (13), and (14), resulting in a map from q and f to i. The error becomes larger for lower frequencies, due to the large gradient in the $P \to i$ map (Fig. 6 upper left). The RMSE is lowest at 1.46% for 50Hz and highest at 5.87% for 20Hz, when compared to $I_{\text{nom}} = 14\text{A}$. We further discuss the achieved accuracy in the following sections 4 and 5.

4. SOFT SENSOR IMPLEMENTATION

We choose an Unscented Kalman filter (UKF) (Julier and Uhlmann, 1997) as the basis for the soft sensor. The model outlined in the previous sections is transformed into a state-space model

$$\frac{\mathrm{d}x_i(t)}{\mathrm{d}t} = \frac{1}{T_c}\left(-x_i(t) + i(\overbrace{U(f)}^{(3)}, \underbrace{\overbrace{P(f,x_q)}^{(13)} - \overbrace{P^-(f,x_q)}^{(14)}}_{(12)})\right)$$

$$\frac{\mathrm{d}x_q(t)}{\mathrm{d}t} = 0 \tag{15}$$

and

$$y(t) = i^*(t) = x_i(t),\ \hat{q}(t) = x_q(t) \tag{16}$$

with augmented state vector $x = (x_i \ x_q)^T$, where x_q equals the estimated flow rate $\hat{q}$ and replaces q in the state equations (15). The augmented state x_q is adjusted by the estimator to achieve convergence of $y(t)$ and measured $i(t)$. We choose tuning matrices

$$Q = \begin{pmatrix} 0.05 & 0 \\ 0 & 0.2 \end{pmatrix}\ ,\ r = 2\ , \tag{17}$$

and the remaining tuning parameters as proposed in Wan and Van Der Merwe (2000). The update of the state with (15) is implemented using the RK4 algorithm. The update rate of the UKF is $T_S = 0.1$ seconds and equals

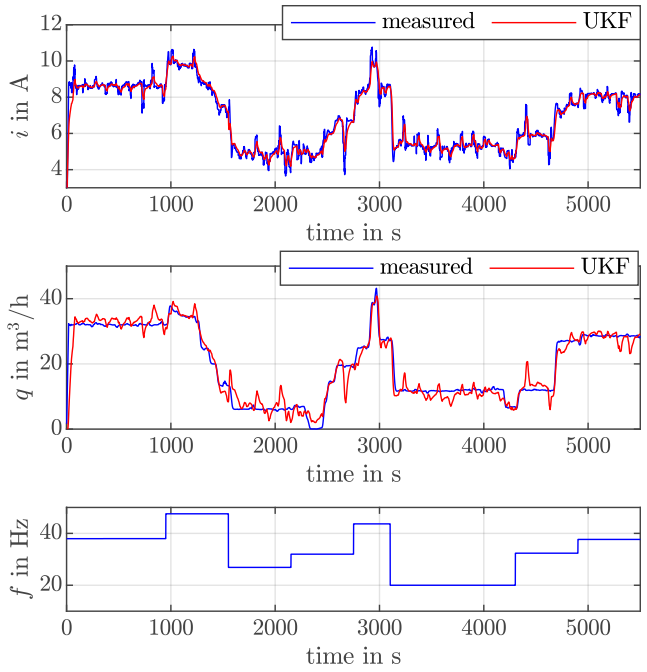

Fig. 7. Test run of the soft sensor.

the sampling rate of the measuring equipment. Figure 7 depicts the results from a test run of the UKF in the laboratory plant from Fig. 5. The upper diagram depicts the primary estimation of i, while the middle diagram depicts the estimation of the desired flow rate q. The lower diagram holds the frequency f, which deliberately changed several times during the recorded interval. The valve opening (cf. Fig. 5) was also changed during the measured interval to vary the downstream flow resistance. The valve opening variation is not recorded but apparent from the flow rate change.

The measured i shows a considerable measurement noise, which is less obvious in the standard deviation of 0.316A, but in a high peak-to-average value of 1.63A. The tuning matrices (17) were chosen concerning this noise, and are a compromise between noise suppression and agility of the $\hat{q}$ estimation.

The resulting $\hat{q}$ follows the true flow rate well, also during the transients. A certain noise is present in $\hat{q}$, resulting from the mentioned compromise in the tuning. The $\hat{q}$ estimation shows a comparable quality for all frequencies recorded in the interval. The RMSE over the whole time series is $2.86\text{m}^3/\text{h}$, or 4.76% relative to $q_{\text{cav}} = 60\text{m}^3/\text{h}$, i.e. the maximal admissible flowrate before cavitation starts.

5. CONCLUSION

We outlined a simplified modeling approach for a centrifugal pump and motor system and evaluated the parameterization process and the model quality in a flow rate soft sensor application. The soft sensor is less precise than a modern hardware flow meter, where deviations of ±1% or less are usually guaranteed. The precision achieved by the soft sensor certainly suffices, however, for nonprecision closed-loop control and efficiency improvement measures. The results support the simplified modeling approach and suggest future activities to enable digital machine twins to incorporate the individual models and thus envision an approach towards a standardized flow rate soft sensor. Future works also include a reliability evaluation of the approach in different setups and a quantification of the errors induced by parameterization and their propagation through the soft sensor.

REFERENCES

Al-Obaidi, A.R. (2019). Investigation of effect of pump rotational speed on performance and detection of cavitation within a centrifugal pump using vibration analysis. *Heliyon*, 5(6).

Allirani, S. (2009). Direct torque control technique for voltage source inverter fed induction motor drive. *International journal of electrical engineering*, 5, 629–640.

Arun Shankar, V.K., Umashankar, S., Paramasivam, S., and Hanigovszki, N. (2016). A comprehensive review on energy efficiency enhancement initiatives in centrifugal pumping system. *Applied Energy*, 181, 495–513.

Benheniche, A. and Bensaker, B. (2015). A high gain observer based sensorless nonlinear control of induction machine. *International Journal of Power Electronics and Drive Systems (IJPEDS)*, 5, 305. doi:10.11591/ijpeds.v5.i3.pp305-314.

Cao, W. and Mao, J. (2019). Study of the affinity law of energy and cavitation characteristics in emergency drainage pumps at different rotating speeds. *Processes*, 7(12), 932.

Doraiswami, R. and Cheded, L. (2014). Robust model-based soft sensor: Design and application. *IFAC Proceedings Volumes*, 47(3), 5491–5496.

Elsey, J. (2023). How to define and measure centrifugal pump efficiency: Part 1. `https://www.pumpsandsystems.com/how-define-measure-centrifugal-pump-efficiency-part-1`. Accessed: 2023-11-08.

Emancipator, K. and Kroll, M.H. (1993). A quantitative measure of nonlinearity. *Clinical chemistry*, 39(5), 766–772.

Gülich, J. (2010). *Centrifugal Pumps*. Springer Berlin Heidelberg.

Julier, S.J. and Uhlmann, J.K. (1997). New extension of the kalman filter to nonlinear systems. In *Signal processing, sensor fusion, and target recognition VI*, volume 3068, 182–193. Spie.

Leonow, S. and Mönnigmann, M. (2013). Soft sensor based dynamic flow rate estimation in low speed radial pumps. In *European Control Conference 2013, Zurich*, 778–783.

Leonow, S. and Mönnigmann, M. (2016). Operating point estimation in hydraulic turbomachines with non-invertible characteristics. In *Proceedings of the European Control Conference 2016 (ECC16), Aalborg*, 2381–2385.

Lima, R.P.G., Mauricio Villanueva, J.M., Gomes, H.P., and Flores, T.K.S. (2022). Development of a soft sensor for flow estimation in water supply systems using artificial neural networks. *Sensors*, 22(8), 3084.

Lin, P., Li, Y., Xu, W., Chen, H., and Zhu, Z. (2020). Numerical study on the influence of inlet guide vanes on the internal flow characteristics of centrifugal pump. *Processes*, 8(1), 122.

Martin, D., Kühl, N., and Satzger, G. (2021). Virtual sensors. *Business & Information Systems Engineering*, 63, 315–323.

Pauly, C.P. (2011). Sensing down to the operating point. *World Pumps*, 2011(9), 32–35.

Schröder, D. (2013). *Fundamentals of Electrical Drives (in German)*. Springer-Lehrbuch. Springer Berlin Heidelberg.

Wan, E.A. and Van Der Merwe, R. (2000). The unscented kalman filter for nonlinear estimation. In *Proceedings of the IEEE 2000 Adaptive Systems for Signal Processing, Communications, and Control Symposium (Cat. No. 00EX373)*, 153–158. Ieee.

Wang, D., Liu, J., and Srinivasan, R. (2009). Data-driven soft sensor approach for quality prediction in a refining process. *IEEE Transactions on Industrial Informatics*, 6(1), 11–17.

Wu, Y., Wu, D., Fei, M., Sørensen, H., Ren, Y., and Mou, J. (2023). Application of ga-bpnn on estimating the flow rate of a centrifugal pump. *Engineering Applications of Artificial Intelligence*, 119, 105738.